Complex scaling calculation of phase shifts for positron collisions with positive ions

Taishi Sano [*]
Department of Chemistry, Tohoku University, Sendai 980-8578, Japan

Takuma Yamashita [†]
Institute for Excellence in Higher Education, Tohoku University, Sendai 980-8576, Japan
and Department of Chemistry, Tohoku University, Sendai 980-8578, Japan

Yasushi Kino
Department of Chemistry, Tohoku University, Sendai 980-8578, Japan

We present phase-shift calculations for positron collisions with positive ions using a complex scaling method (CSM) in which the phase shifts are derived only from the complex eigenenergies of the CSM Hamiltonian. Based on the findings of this study [R. Suzuki, T. Myo, and K. Katō, Prog. Theor. Phys. **113**, 1273 (2005)], we propose a modification of the phase shift in the CSM calculation for application to few-body scattering problems. This modification is based on the fact that the contributions of high-lying complex eigenenergies to the phase shift can be approximated as a constant value in the case of small collision energy, where neither target excitation nor positronium formation occurs. The proposed modification limits the contribution of the complex eigenenergies to the vicinity of the collision energy, which is intuitively acceptable. We present a geometrical formulation of the modification and demonstrative calculations of positron scattering off positive ions. Our results agree well with those reported in the literature for the targets Ne, Ar, Kr, Xe, H, He, He$^+$, and Li^{2+}. The phase shifts of positron scattering off a Li$^+$ ion are also reported.

I. INTRODUCTION

An observation of a positron scattering off an atom provides essential insights into the behavior of positrons in matter. Positrons interact attractively with electrons comprising the target atom and can form a positronium (Ps) atom, which is a bound state of the electron and positron. Even when the collision energy is below the threshold for Ps formation, it is crucial to consider virtual Ps formation during the scattering process, which results in a challenging two-center problem and requires rigorous theoretical treatment [1,2]. In recent years, the improvement in the positron beam quality [3,4] revealed scattering cross sections with a variety of atoms or molecules over a wide range of collision energies [5–7]. Furthermore, the development of Ps beams [8–11] has stimulated interest in positronium-atom interactions [12–18].

Compared to positron scattering off neutral atoms, the investigation of the scattering off positive ions has been relatively limited. This is due to the experimental difficulties and theoretical complexities arising from the long-range Coulomb repulsion between the positron and ion. For instance, positron scattering off a He$^+$ ion has been studied using various theoretical approaches [19–22] for a considerable time, and

the latest calculations [22] confirmed the accuracy and provided a valuable benchmark for theoretical approaches.

The complex scaling method (CSM) has been widely used to calculate the resonance energies and widths of various few-body systems [23] while its application to the nonresonant scattering problems has been relatively limited. Suzuki *et al.* [24–27] proposed a CSM calculation of phase shifts by investigating the relationship among the complex eigenenergies of the CSM Hamiltonian, continuum level density (CLD), and scattering matrices. In the CSM calculation of the phase shifts, once the complex eigenenergies of the CSM Hamiltonian are obtained, the phase shifts can be calculated as smooth functions of collision energies. The CSM basis functions are square integrable functions that damp out within a finite space. This advantage contrasts with other conventional approaches that utilize an explicit form of the scattering wave function and require individual calculations for each collision energy.

In this study, we demonstrate the effectiveness of the CSM calculation for low-energy positron scattering off positive ions, where the collision energy is lower than the first excitation energy of the target atom or ion. To the best of our knowledge, this CSM approach has not been applied to the phase-shift calculations of atomic or molecular systems and can be used as an alternative approach to atomic and molecular scattering problems, including those involving positrons.

To demonstrate the validity of the CSM, we examine the positron collision with noble gas atoms, treating it as a two-body problem using model potentials. We then investigate

---

[*]Present address: Department of Physics, Waseda University, Shinjuku 169-8050, Japan.
[†]tyamashita@tohoku.ac.jp

the roles of the eigenenergies responsible for determining the phase-shift behavior of low-energy scattering. We consider the empirical fact that numerical convergence requires a large set of complex eigenenergies even in the case of low-energy scattering. The majority of the complex eigenenergies have a large real part compared to the small collision energy, which is counterintuitive. To calculate the phase shift using a finite set of eigenenergies, we propose an effective modification for low-energy scattering. We apply the CSM to positron scattering off a helium ion (He$^+$), hydrogen atom (H), and lithium ion (Li^{2+}) as examples of a three-body problem. We employ the Gaussian expansion method [28] and accurately describe the interparticle interactions. We then perform analogous computations for four-body systems, namely, positron scattering off a He atom and Li$^+$ ion.

The remainder of this paper is organized as follows. In Sec. II, we provide an overview of the CSM-based calculation of the continuum-level density and phase shift. Subsequently, we describe the basis functions for the calculation of positron-atom scattering. In Sec. III, we highlight a case study of e$^+$-Ne scattering and examine the problems in the convergence behavior of low-energy phase shifts. Subsequently, we propose a modification for low-energy scattering phase shifts and demonstrate the modification for e$^+$-X (X = Ne, Ar, Kr, Xe) scattering, e$^+$-X (X = H, He$^+$, Li^{2+}) three-body scattering, and e$^+$-X (X = He, Li$^+$) four-body scattering. Finally, the conclusions are summarized in Sec. IV.

Atomic units (a.u.; $m_e = \hbar = e = 1$) are used throughout this study, except where otherwise mentioned. The Bohr radius is denoted as a_B.

II. THEORY

A. Phase-shift calculation with complex scaling method

The framework of the phase-shift calculation using CSM is presented in Refs. [24–27]. Here, we briefly describe the outline of the formulation, which is important for the following discussion.

We consider a Hamiltonian H consisting of a kinetic energy operator T and a potential energy operator V. In the CSM, all the coordinates are applied to $\exp(i\theta)$ as follows:

$$\boldsymbol{r} \rightarrow \exp(i\theta)\boldsymbol{r}, \tag{1}$$

where θ is a real number and i is an imaginary unit. Using the CSM, the Schrödinger equation for the complex-scaled Hamiltonian is written as

$$H(\theta)\Psi(\theta) = E(\theta)\Psi(\theta), \tag{2}$$

where the wave function $\Psi(\theta)$ is associated with the eigenenergy $E(\theta)$, which is a complex value because the Hamiltonian is no longer Hermitian. If the wave function $\Psi(\theta)$ is expanded in terms of a finite number $N_{\max}$ of L^2 integrable basis functions, $E(\theta)$ takes discrete energies $E_k(\theta)(k = 1, \ldots, N_{\max})$ by a diagonalization of the complex scaled Hamiltonian as

$$\langle \tilde{\Psi}_{k'}(\theta)|H(\theta)|\Psi_k(\theta)\rangle = E_k(\theta)\delta_{k'k}, \tag{3}$$

where the bra states with $\tilde{\Psi}_k$ denote the biorthogonal state of the ket state. The continuum states then become discrete states, which are referred to as called pseudostates.

The $E_k(\theta)$ of the bound state does not change with a change in θ. In contrast, the $E_k(\theta)$ of the scattering state (pseudostates) almost rotates by -2θ in the complex energy plane because the kinetic energy operator T of the Hamiltonian is expressed as $\exp(-2i\theta)T$ in the complex scaled Hamiltonian. The $E_k(\theta)$ of a resonance state approaches a complex resonance energy, and the real and imaginary parts of which represent the resonance energy and width, respectively. The eigenfunctions $\{\Psi_k(\theta)\}$ satisfy the completeness relation [29,30] approximately as follows:

$$\sum_{k=1}^{N_{\max}} |\Psi_k(\theta)\rangle \langle \tilde{\Psi}_k(\theta)| \approx 1. \tag{4}$$

In this work, we calculate the scattering phase shift $\delta(E)$ based on the continuum level density (CLD) that is defined as [31,32]

$$\mathcal{D}(E) = -\frac{1}{\pi}\text{Im}\{\text{Tr}[G^+(E) - G_0^+(E)]\}, \tag{5}$$

where $G^+(E) = (E + i\varepsilon - H)^{-1}$ and $G_0^+(E) = (E + i\varepsilon - H_0)^{-1}$ are the full and free Green's functions, respectively. H denotes the full Hamiltonian of the system and H_0 is an asymptotic form of the full Hamiltonian.

The CLD $\mathcal{D}(E)$ is related to the scattering matrix $S(E)$ as [25,32–34]

$$\mathcal{D}(E) = \frac{1}{2\pi}\text{Im}\frac{d}{dE}\ln \det S(E). \tag{6}$$

When the asymptotic interaction between the collision fragments does not include an explicit Coulomb potential energy operator, the H_0 only contains kinetic energy operators along with the relative coordinate between the fragments and internal Hamiltonians of the collision fragments. In this case, the $S(E)$ calculated from $\mathcal{D}(E)$ by Eq. (6) corresponds to an amplitude of the outgoing spherical Hankel function. For the case where the both collision fragments have nonzero charges, we include the asymptotic Coulomb potential energy operator in H_0 so that the scattering matrix $S(E)$ corresponds to the amplitude of the outgoing spherical Coulomb function. The H and H_0 used in this paper are presented in the following sections, see Eqs. (14), (18), and (21).

For a single-channel (elastic) scattering problem, because $\det S(E) = \exp[2i\delta(E)]$, where $\delta(E)$ denotes the phase shift, the phase shift is obtained from the CLD as

$$\delta(E) = \int_{-\infty}^{E} \mathcal{D}(E')dE'. \tag{7}$$

Using the completeness relation of Eq. (4), the $\mathcal{D}(E)$ in Eq. (5) is rewritten as

$$\mathcal{D}(E) \approx -\frac{1}{\pi}\text{Im}\left[\sum_{k=1}^{N_{\max}} \frac{1}{E + i\epsilon - E_k(\theta)} - \sum_{k=1}^{N_{\max}} \frac{1}{E + i\epsilon - E_{0,k}(\theta)}\right], \tag{8}$$

where the summation over k runs for all the eigenenergies, $k = 1, \ldots, N_{\max}$, obtained by the full diagonalization of the Hamiltonian with the $N_{\max}$ basis functions according to

Eq. (3). The $\{E_k\}$ and $\{E_{0,k}\}$ are the eigenenergies of $H(\theta)$ and $H_0(\theta)$, respectively, and are obtained using the *same* basis functions.

In the case of single-channel scattering, Eqs. (7) and (8) provide simple expressions for the phase shift

$$\delta(E_{\mathrm{col}}) = \left[\sum_{k=1}^{N_{\max}} \delta_k(E_{\mathrm{col}}) - \sum_{k=1}^{N_{\max}} \delta_{0,k}(E_{\mathrm{col}}) \right], \qquad (9)$$

where

$$\delta_k(E_{\mathrm{col}}) = \tan^{-1}\left(\frac{-\mathrm{Im}E_k(\theta)}{\mathrm{Re}E_k(\theta) - E_{\mathrm{col}}} \right), \qquad (10)$$

and

$$\delta_{0,k}(E_{\mathrm{col}}) = \tan^{-1}\left(\frac{-\mathrm{Im}E_{0,k}(\theta)}{\mathrm{Re}E_{0,k}(\theta) - E_{\mathrm{col}}} \right). \qquad (11)$$

It should be noted that, on the complex energy plane, $\delta_{(0,)k}(E_{\mathrm{col}})$ corresponds to the angle of depression of $E_{(0,)k}(\theta)$, as measured from the real energy E_{col}. Thus, the calculation of the phase shift $\delta(E_{\mathrm{col}})$ is reduced to the sum of the geometrical angles of the complex eigenenergies on the complex energy plane.

B. Two-body systems: e^+-X (X = Ne, Ar, Kr, Xe)

We consider noble gas atom (X = He, Ar, Kr, or Xe) targets as a simple positron scattering problem. As atoms have a closed-shell structure and the kinetic energy of the positron is less than the excitation energy, a two-body model is used in the study. The Hamiltonian H can be written as follows:

$$H_{\mathrm{2bd}} = \frac{\boldsymbol{p}^2}{2\mu_{\mathrm{e}}} + V_{e^+X}(r), \qquad (12)$$

where r denotes the distance between e^+ and the center of mass of the noble gas atom X, and $\boldsymbol{p}$ is the momentum operator along with the vector $\boldsymbol{r}$. μ_{e} denotes the reduced mass between e^+ and X. $V_{e^+X}(r)$ is a model potential that describes the static Coulomb repulsion and induced dipole polarization as

$$V_{e^+X}(r) = \frac{Z}{r} \sum_i^N A_i e^{-\alpha_i r} - \frac{\alpha_{\mathrm{d}}}{2r^4}(1 - e^{-(r/r_c)^6}). \qquad (13)$$

Here, the static potential parameters $\{A_i\}$ and $\{\alpha_i\}$ are obtained to reproduce the elastic cross section and are given in Refs. [35,36] for Ne, Ar, and Xe and Ref. [35] for Kr. The induced polarization potential parameters α_{d} and r_c are obtained from Ref. [36] for Ne, Ar, and Xe and Ref. [37] for Kr. For these systems, we define the reference Hamiltonian H_0 using only the kinetic energy operator

$$H_{0,\mathrm{2bd}} = \frac{\boldsymbol{p}^2}{2\mu_{\mathrm{e}}}. \qquad (14)$$

According to Eq. (3), we diagonalize H_{2bd} and $H_{0,\mathrm{2bd}}$ using Gaussian basis functions as follows:

$$\psi_{klm}(\mathbf{r}) = \sum_{i=1}^{n_b} C_i^{(k)} r^l e^{-b_i r^2} Y_{lm}(\hat{\mathbf{r}}), \qquad (15)$$

where the nonlinear Gaussian range parameters $\{b_i; i = 1, 2, \ldots, n_b\}$ (real values) are selected in accordance with the
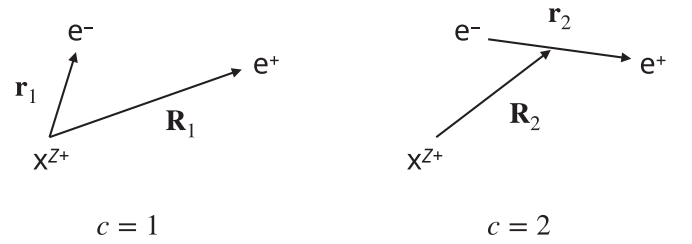

FIG. 1. Two sets of coordinates in e^+-H/He$^+$/Li^{2+} scattering.

geometrical progression. l and m are azimuthal and magnetic quantum numbers, respectively. The linear coefficients $\{C_i^{(k)}\}$ are determined using the Rayleigh-Ritz variational method for the complex scaling Schrödinger equation such that ψ_{klm} satisfies the following condition:

$$\langle \tilde{\psi}_{k'lm}(\theta)|H_{\mathrm{2bd}}(\theta)|\psi_{klm}(\theta) \rangle = E_k(\theta)\delta_{kk'}. \qquad (16)$$

For the asymptotic Hamiltonian $H_{0,\mathrm{2bd}}$, as in the case of Eq. (16), we obtain the eigenenergies $\{E_{0k}\}$. We typically use $n_b = 60$ and $0.01 \leqslant 1/\sqrt{b_i} \leqslant 300\, a_{\mathrm{B}}$.

C. Three-body systems: e^+-X (X = H, He$^+$, Li^{2+})

As a second example of positron scattering, we consider e^+-X (X = H, He$^+$, Li^{2+}) scattering in a three-body treatment. These systems consist of three distinguishable particles, e^+, e^-, and x^{Z+} (the nucleus of X). Assuming an infinite mass of X, the three-body Hamiltonian can be written as

$$H_{\mathrm{3bd}} = \frac{\boldsymbol{p}_{e^-}^2 + \boldsymbol{p}_{e^+}^2}{2} - \frac{Z}{r_{e^-}} + \frac{Z}{r_{e^+}} - \frac{1}{r_{e^+e^-}}, \qquad (17)$$

where $r_{e^-(e^+)}$ denotes the distance between the X and $e^-(e^+)$, and Z is the atomic number of the nucleus. $r_{e^+e^-}$ is the distance between e^- and e^+. For the cases X = He$^+$ and Li^{2+}, owing to the repulsive Coulomb interaction remaining in the asymptotic distance, the corresponding asymptotic Hamiltonian $H_{0,\mathrm{3bd}}$ is generally expressed as
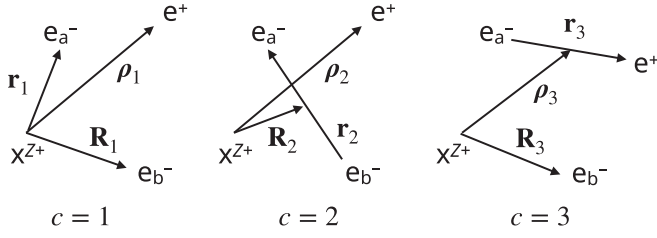
$$H_{0,\mathrm{3bd}} = \frac{\boldsymbol{p}_{e^-}^2 + \boldsymbol{p}_{e^+}^2}{2} - \frac{Z}{r_{e^-}} + \frac{Z-1}{r_{e^+}}, \qquad (18)$$

where the first term of the potential energy operators, $-Z/r_{e^-}$, provides a correct threshold energies of collision fragments and the second term, $(Z-1)/r_{e^+}$, provides the asymptotic repulsive Coulomb interaction between the collision fragments for $Z > 1$ cases.

The wave function of the three-body system is written as

$$\begin{aligned}\Psi_{kJM} = \sum_{c=1}^{2} \sum_{l,L} \sum_{i} &\left(C_{clLi}^{(k)} \cos\left(\beta \nu_{clLi} R_c^2 \right) \right. \\ &+ \left. D_{clLi}^{(k)} \sin\left(\beta \nu_{clLi} R_c^2 \right) \right) r_c^l R_c^L \\ &\times \exp\left(-\mu_{clLi} r_c^2 - \nu_{clLi} R_c^2 \right)[Y_l(\hat{\boldsymbol{r}}_c) \otimes Y_L(\hat{\boldsymbol{R}}_c)]_{JM},\end{aligned} \qquad (19)$$

where the coordinate sets $(\boldsymbol{r}_1, \boldsymbol{R}_1) = (\boldsymbol{r}_{e^-}, \boldsymbol{r}_{e^+})$ and $(\boldsymbol{r}_2, \boldsymbol{R}_2) = (\boldsymbol{r}_{e^-e^+}, \boldsymbol{R})$ are presented in Fig. 1. The parameters $\{\nu_{clLi}\}$ and $\{\mu_{clLi}\}$ are selected in accordance with the geometrical progression. The typical ranges are $0.01 \leqslant 1/\sqrt{\mu_{clLi}} \leqslant 20\, a_{\mathrm{B}}$ and $0.05 \leqslant 1/\sqrt{\nu_{clLi}} \leqslant 80\, a_{\mathrm{B}}$. The two spherical harmonics
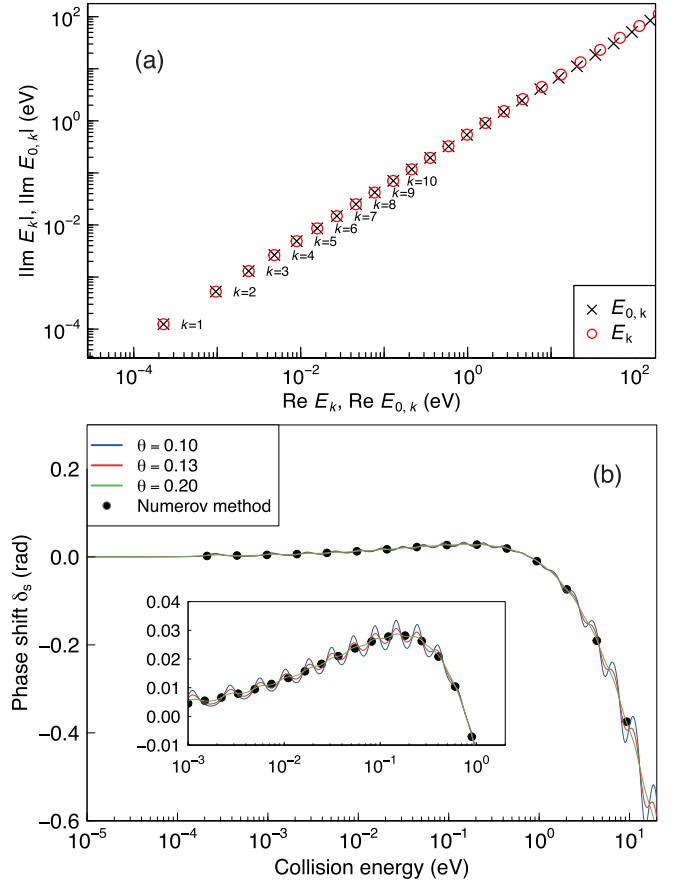
FIG. 2. Three sets of coordinates in e^+-He^+ scattering.

FIG. 3. (a) Complex eigenenergies $\{E_k\}$ and $\{E_{0,k}\}$ calculated for $e^+ + Ne$ at the complex scaling parameter $\theta = 0.25$. (b) Convergence of the S-wave phase shift of $e^+ + Ne$ scattering against complex scaling parameters $\theta = 0.10$ (most oscillating curve), 0.13, and 0.25 (most smooth curve). The phase shifts are compared with those calculated using the Numerov method. The inset is a close-up view of the phase shift behavior in the vicinity of 10^{-2}-10^0 eV.

are coupled to provide the total angular momentum J and its projection onto the z axis, M. The parameter $\beta = 1.5$ introduces oscillations in the Gaussian functions and increases the orthogonality of the basis functions. Linear coefficients $C^{(k)}_{clLi}$ and $D^{(k)}_{clLi}$ are determined by the diagonalization as in Eq. (3). The eigenenergies $\{E_k\}$ and $\{E_{0k}\}$ are obtained in a manner similar to that in Eq. (16).

D. Four-body systems: e^+-X (X = He, Li$^+$)

Similar to Sec. II C, the four-body Hamiltonian for e^+-X (X = He, Li$^+$) scattering is expressed as

$$
H_{4bd} = \frac{p^2_{e^-_a} + p^2_{e^-_b} + p^2_{e^+}}{2} - \frac{Z}{r_{e^-_a}} - \frac{Z}{r_{e^-_b}} + \frac{1}{r_{e^-_a e^-_b}} + \frac{Z}{r_{e^+}} - \frac{1}{r_{e^+ e^-_b}} - \frac{1}{r_{e^+ e^-_b}}, \tag{20}
$$

where the two electrons are labeled as e^-_a and e^-_b. The asymptotic Hamiltonian $H_{0,4bd}$ is defined assuming the distances between the positron and the other particles approach the same distances represented by r_{e^+}, i.e.,

$$
H_{0,4bd} = \frac{p^2_{e^-_a} + p^2_{e^-_b} + p^2_{e^+}}{2} - \frac{Z}{r_{e^-_a}} - \frac{Z}{r_{e^-_b}} + \frac{1}{r_{e^-_a e^-_b}} + \frac{Z-2}{r_{e^+}}. \tag{21}
$$

The wave function of the four-body system is written as

Ψ_{kJM}

$$
= \sum_{c=1}^{3} \sum_{l,L,\lambda} \sum_{i} \left(C^{(k)}_{clL\lambda i} \cos\left(\beta v_{clLi} \rho^2_c\right) + D^{(k)}_{clL\lambda i} \sin\left(\beta v_{clLi} \rho^2_c\right) \right)
$$
$$
\times r^l_c R^L_c \rho^\lambda_c \exp\left(-\mu_{clL\lambda i} r^2_c - v_{clL\lambda i} R^2_c - \zeta_{clL\lambda i} \rho^2_c\right)
$$
$$
\times [[Y_l(\hat{r}_c) \otimes Y_L(\hat{R}_c)]_\Lambda \otimes Y_\lambda(\hat{\rho}_c)]_{JM} + (a \leftrightarrow b), \tag{22}
$$

where the coordinate sets $(r_c, R_c, \rho_c) = (r_{e^-}, r_{e^+})$ are presented in Fig. 2. The last term $a \leftrightarrow b$ is an electron-permutated basis function because we consider the electronic spin singlet state and space-symmetric wave functions throughout this paper. The nonlinear parameters are selected in a manner similar to that of the three-body problem. Linear coefficients $C^{(k)}_{clL\lambda i}$ and $D^{(k)}_{clL\lambda i}$ are determined by the diagonalization as in Eq. (3).

III. RESULTS AND DISCUSSION

A. Case study of potential scattering of e^+-Ne collision

We begin the discussion with a case study of e^+-Ne scattering. Using 60 Gaussian basis functions as described in Sec. II B, the 60 complex eigenenergies $\{E_k\}$ and $\{E_{0,k}\}$ are obtained for complex-scaled Hamiltonians H_{2bd} and $H_{0,2bd}$, respectively. Figure 3(a) presents the lowest 23 eigenenergies calculated with the complex scaling parameter $\theta = 0.25$ for S-wave scattering. The system has no bound or resonance states, and all eigenenergies obtained are attributed to continuum states. Figure 3(b) presents the S-wave phase shifts calculated for several complex scaling angles: $\theta = 0.10, 0.13$, and 0.25. To verify our calculations, we calculated the phase shifts using the Numerov method with high precision. The phase shift realized using a small complex scaling parameter, e.g., $\theta = 0.10$, exhibits an oscillation around the exact phase shift obtained using the Numerov method. By increasing the scaling angle, the oscillation is reduced and converges to an exact value. The calculation of $\theta = 0.25$ produces almost the same phase shift as that obtained using the Numerov method below the first excitation energy of Ne. For a small
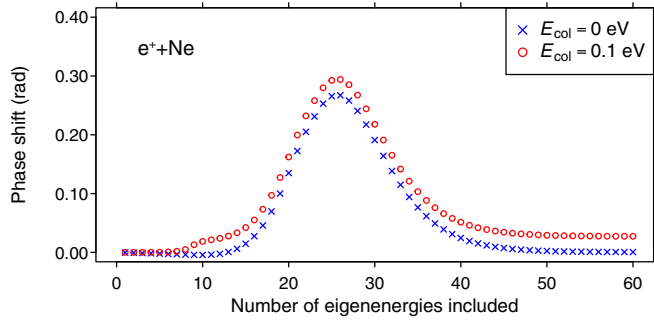
FIG. 4. Convergence of the S-wave phase shift $\delta^{(n)}(E_{\mathrm{col}})$ [see Eq. (23) for definition] of e^+-Ne at $E_{\mathrm{col}} = 0$ and 0.1 eV against the number of eigenenergies included n.

collision energy, the phase shift increases as the collision energy increases and then decreases, thus crossing zero at approximately $E_{\mathrm{col}} = 0.8$ eV. This behavior results in a minimum S-wave cross section and a minimum total cross section, which is known as the Ramsauer-Townsend effect [36].

B. Problems in convergence behavior of low-energy phase shift

In Sec. III A, we confirmed that the phase-shift calculation performed using all ($N_{\max} = 60$ in this case) eigenenergies provides an accurate result for the e^+-Ne scattering when the complex scaling angle θ is sufficiently large. In this section, we examine the convergence of the phase shift against the number of eigenenergies included. This consideration is crucial when we calculate three-body and four-body scattering problems.

As observed in Fig. 3(a), the eigenenergies $\{E_k\}$ are close to $\{E_{0,k}\}$. Thus, we can sort these eigenenergies by $\mathrm{Re}\, E_{(0,)k}$ in ascending order and truncate Eq. (9) as

$$\delta^{(n)}(E_{\mathrm{col}}) := \sum_{k=1}^{n} [\delta_k(E_{\mathrm{col}}) - \delta_{0,k}(E_{\mathrm{col}})], \qquad (23)$$

where $n \leqslant N_{\max}$. Figure 4 illustrates the e^++Ne scattering phase shift $\delta^{(n)}(E_{\mathrm{col}})$ as a function of n. According to Levinson's theorem, the exact phase shift $\delta(E_{\mathrm{col}} = 0\,\mathrm{eV})$ is zero. As shown in Sec. III A, $\delta^{(n=N_{\max})}(E_{\mathrm{col}} = 0\,\mathrm{eV})$ is reproduced to zero. However, the convergence behavior of $\delta^{(n)}(E_{\mathrm{col}})$ is not trivial; $\delta^{(n)}(E_{\mathrm{col}} = 0\,\mathrm{eV})$ first increases as the number of eigenenergies included in (n) increases. $\delta^{(n)}(E_{\mathrm{col}})$ decreases and finally converges to zero. A similar trend was observed for $\delta^{(n)}(E_{\mathrm{col}} = 0.1\,\mathrm{eV})$ although the converged phase shift is not zero. This indicates that we require almost all the eigenenergies having real parts much larger than the collision energy E_{col}. For example, in the present case, $\mathrm{Re}\, E_{k=25} \approx 250$ eV, which is counterintuitively larger than E_{col}.

This "slow" convergence against n of the truncated phase shift $\delta^{(n)}(E_{\mathrm{col}})$ causes a problem in its application to few-body scattering. We demonstrate the calculation of $e^+ + He^+$ scattering as a typical case of few-body problems. Figure 5(a) presents the complex eigenenergies of a three-body system (e^+, e^-, and He^{2+}), which are obtained by diagonalization with approximately 4500 basis functions. Because of the internal energy of $He^+(1s)$ $E_{He^+(1s)} = -54.4\,\mathrm{eV}$, the lowest $\{E_k\}$ and $\{E_{0,k}\}$ values are located just above the threshold energy
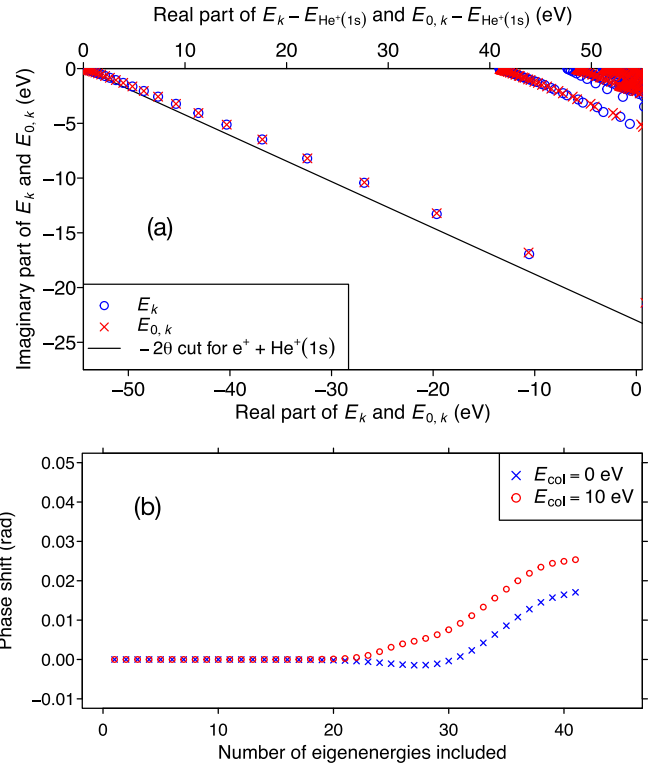

FIG. 5. (a) Complex eigenenergies $\{E_k\}$ and $\{E_{0,k}\}$ calculated for $e^+ + He^+$ at the complex scaling parameter $\theta = 0.20$. (b) Convergence of the S-wave phase shift $\delta^{(n)}(E_{\mathrm{col}})$ of $e^+ + He^+$ at $E_{\mathrm{col}} = 0$ and 10 eV against the number of eigenenergies included n.

-54.4 eV. In contrast to the two-body problem of e^++Ne scattering, the eigenenergies at high energies cannot be attributed to any of the specific physical channels because there are several inelastic channels, and the corresponding eigenfunction must be a multichannel scattering wave function. In the present case, we observe a series of eigenenergies that rotate by 2θ around the lowest threshold energy $e^+ + He^+(1s)$. Taking these complex eigenenergies into consideration, we examine the convergence of $\delta^{(n)}(E_{\mathrm{col}})$, as shown in Fig. 5(b). Although we include eigenenergies having real parts exceeding 40 eV, $\delta^{(n)}(E_{\mathrm{col}} = 0\,\mathrm{eV})$ and $\delta^{(n)}(E_{\mathrm{col}} = 10\,\mathrm{eV})$ do not reach convergence. At least $\delta^{(n)}(E_{\mathrm{col}} = 0\,\mathrm{eV})$ should converge to zero, while $\delta^{(n=40)}(E_{\mathrm{col}} = 0\,\mathrm{eV})$ deviates significantly from zero.

C. Modification to the low-energy phase shift

In this subsection, we discuss the effective modification of the low-energy scattering phase shift when the number of eigenenergies is limited. As observed in the convergence behavior of $\delta^{(n)}(E_{\mathrm{col}})$, the high-lying eigenenergies contributed to the determination of the low-energy phase shift. For practical purposes in atomic physics, it is worth proposing an effective modification to calculate low-energy phase shift even when only a limited number of eigenenergies close to the E_{col} are obtained. The phase shift is obtained by summing the angles of depression of $E_{(0,)k}$ measured from E_{col}; therefore, the contributions from the high-lying eigenenergies are expected
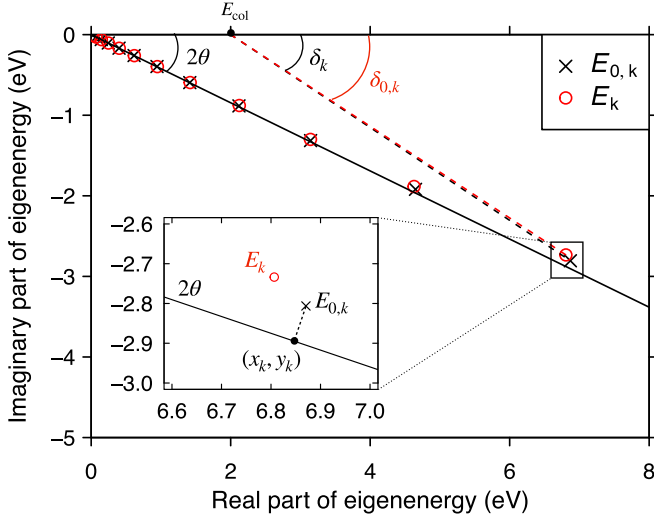
FIG. 6. Schematic of complex eigenenergies and the related angles of depression on the complex energy plane. (x_k, y_k) is selected as the closest point to $E_{0,k}$ on the 2θ line.

to be insensitive to changes in E_{col} in the low-energy scattering region.

Thus, we formulate the contributions from the high-lying eigenenergies to the phase shift, with particular emphasis on the E_{col} dependency. We consider a situation wherein the eigenenergies $\{E_k\}$ are observed close to $\{E_{0,k}\}$ and can define eigenenergy pairs $(E_k, E_{0,k})$ as illustrated in Fig. 6. Each eigenenergy pair causes the following angular difference:

$$\delta_{\text{diff},k}(E_{col}) := \delta_k(E_{col}) - \delta_{0,k}(E_{col}). \quad (24)$$

The sum of which over k yields a phase shift $\delta(E_{col})$. It should be noted that, in Fig. 6, $\{E_{0,k}\}$ are not exactly on the 2θ cut owing to the asymptotic Coulomb potential operator contained in H_0 and/or the numerical accuracy, depending on the number and types of basis functions.

We define a point (x_k, y_k) on 2θ cut as $y_k = -\tan(2\theta)x_k$ such that the distance between (x_k, y_k) and $E_{0,k}$ is minimized (see the inset of Fig. 6). Then, E_k and $E_{0,k}$ are expressed as deviations from the same point (x_k, y_k) as follows:

$$(\text{Re } E_k, \text{Im } E_k) =: (x_k(1 + \Delta_{x,k}), y_k(1 + \Delta_{y,k})), \quad (25)$$

and

$$(\text{Re } E_{0,k}, \text{Im } E_{0,k}) =: (x_k(1 + \Delta_{0x,k}), y_k(1 + \Delta_{0y,k})), \quad (26)$$

where $\Delta_{x,k}$, $\Delta_{y,k}$, $\Delta_{0x,k}$, and $\Delta_{0y,k}$ are dimensionless real numbers. Using $\Delta_{x,k}$ and $\Delta_{y,k}$, the arctangent argument in Eq. (10) can be written as

$$\frac{-\text{Im}E_k(\theta)}{\text{Re}E_k(\theta) - E_{col}} = \tan 2\theta \frac{1 + \Delta_{y,k}}{1 + \Delta_{x,k} - E_{col}/x_k}, \quad (27)$$

and a similar expression can be obtained in Eq. (26).

We now consider the case wherein $\Delta_{x,k}$, $\Delta_{y,k} \ll 1$, and $E_{col} \ll x_k$, i.e., the eigenenergy pairs that are located in a significantly high-energy region compared with E_{col}. For brevity, we rewrite

$$\tilde{\Delta}_{x,k} := \Delta_{x,k} - E_{col}/x_k. \quad (28)$$

On expanding $(1 + \tilde{\Delta}_{x,k})^{-1}$ in Eq. (27) and then expanding Eq. (10), $\delta_k(E_{col})$ can be written as a perturbation expansion as (see the Appendix for details)

$$\delta_k(E_{col}) = 2\theta + \frac{1}{2}\sin(4\theta)\{-\tilde{\Delta}_{x,k} + \Delta_{y,k} + \cos^2(2\theta)\tilde{\Delta}_{x,k}^2$$
$$- \cos(4\theta)\tilde{\Delta}_{x,k}\Delta_{y,k} - \sin^2(2\theta)\Delta_{y,k}^2\} + O_3, \quad (29)$$

where O_3 denotes the third-order term of the deviations, $\tilde{\Delta}_{x,k}^3$, $\tilde{\Delta}_{x,k}^2\Delta_{y,k}$, $\tilde{\Delta}_{x,k}\Delta_{y,k}^2$, and $\Delta_{y,k}^3$. Similar expansions can be observed in Eq. (11). Therefore, $\delta_{\text{diff},k}(E_{col})$ in Eq. (24) can be expressed as

$$\delta_{\text{diff},k}(E_{col}) = \frac{1}{2}\sin(4\theta)\{-\tilde{\Delta}_{x,k} + \tilde{\Delta}_{0x,k} + \Delta_{y,k} - \Delta_{0y,k}$$
$$+ \cos^2(2\theta)(\tilde{\Delta}_{x,k}^2 - \tilde{\Delta}_{0x,k}^2)$$
$$- \sin^2(2\theta)(\Delta_{y,k}^2 - \Delta_{0y,k}^2)$$
$$- \cos(4\theta)(\tilde{\Delta}_{x,k}\Delta_{y,k} - \tilde{\Delta}_{0x,k}\Delta_{0y,k})\} + O_3, \quad (30)$$

where $\tilde{\Delta}_{0x(y),k} := \Delta_{0x(y),k} - E_{col}/x_k$.

Because the collision-energy dependence of $\delta_{\text{diff},k}(E_{col})$ emerges from E_{col}/x_k, which appears for every $\tilde{\Delta}_{x(y),k}$ and $\tilde{\Delta}_{0x(y),k}$, the first-order terms in Eq. (30) only contain the term of E_{col}^0, and the second-order term contains only the term E_{col}^0 and E_{col}^1. In summary, $\delta_{\text{diff},k}(E_{col})$ can be written as

$$\delta_{\text{diff},k}(E_{col}) = a_k + \frac{b_k}{x_k}E_{col} + O_3, \quad (31)$$

where a_k and b_k are independent of E_{col} and depend only on the complex scaling angle θ and the parameters of the eigenenergy pairs $\Delta_{x,k}$, $\Delta_{0x,k}$, $\Delta_{y,k}$, and $\Delta_{0y,k}$. From Eq. (31), the second term can be neglected for the eigenenergy pairs with $|x_k| \gg E_{col}$. As $x_x \approx \text{Re } E_{0,k}$, $\delta_{\text{diff},k}(E_{col})$ can be considered a *constant* for a large value of $\text{Re } E_{0,k}$. We then approximate the sum of $\delta_{\text{diff},k}(E_{col})$ originating from the high-lying (large k) complex eigenenergies as constants, the phase shift of the collision energy E_{col} can be expressed as

$$\delta(E_{col}) \approx \sum_{k=1}^{n} \delta_{\text{diff},k}(E_{col}) + \delta_{>n,\text{const.}}. \quad (32)$$

Although $\delta_{>n,\text{const.}}$ is not known in advance, Eq. (32) is valid for $E_{col} = 0$ and Levinson's theorem for a system with no bound state

$$\delta(E_{col} = 0) = 0, \quad (33)$$

provides a constraint. On subtracting Eq. (32) by that of $E_{col} = 0$, we obtain

$$\delta(E_{col}) \approx \sum_{k=1}^{n} [\delta_{\text{diff},k}(E_{col}) - \delta_{\text{diff},k}(E_{col} = 0)]$$
$$= \delta^{(n)}(E_{col}) - \delta^{(n)}(E_{col} = 0). \quad (34)$$

Thus, even when we obtain a limited number of eigenenergy pairs $n < N_{max}$, the subtraction of $\delta^{(n)}(E_{col} = 0)$ from $\delta^{(n)}(E_{col})$ is expected to improve the accuracy of the phase-shift determination. Hereinafter, we refer to the modification

of Eq. (34) as the "calibration." We apply Eq. (34) to several positron-scattering problems in the following subsections.

It would be practically useful to show a way estimating the applicable energy range of the calibration by Eq. (34). The $\delta_{\text{diff},k}(E_{\text{col}})$, the $|a_k x_x/b_k|$ of which satisfies $E_{\text{col}} \ll |a_k x_x/b_k|$ can be considered as a constant with respect to changes in E_{col} under low-energy scattering. The truncation number n should be sufficiently large, such that $\operatorname{Re} E_{(0,)n}$ covers E_{col}. Because (x_k, y_k) is selected as the point closest to $E_{0,k}$ on the 2θ-cut, x_k can be approximated as $\operatorname{Re} E_{0,k}$. Thus, by replacing x_k with $\operatorname{Re} E_{0,k}$, we obtain

$$
\left| \frac{a_k \operatorname{Re} E_{0,k}}{b_k} \right|
$$
$$
\approx \left| \frac{\{(\Delta_{x,k} - \Delta_{0x,k}) - (\Delta_{y,k} - \Delta_{0y,k})\} \operatorname{Re} E_{0,k}}{2\cos^2(2\theta)(\Delta_{x,k} - \Delta_{0x,k}) - \cos(4\theta)(\Delta_{y,k} - \Delta_{0y,k})} \right|.
$$
(35)

Here, the second-order term in a_k is ignored. When the complex scaling angle θ is small (typically $\theta \sim \pi/12$) because $2\cos^2(2\theta) \sim 2(1 - 2\theta)^2 \sim 2(1 - 4\theta)$ and $\cos(4\theta) \sim (1 - 4\theta)$, we obtain the following approximate estimation:

$$
\left| \frac{a_k \operatorname{Re} E_{0,k}}{b_k} \right| \gtrsim \frac{\operatorname{Re} E_{0,k}}{2}.
$$
(36)

Thus, the applicable energy range for Eq. (34) is approximately half that of $\operatorname{Re} E_{0,n}$.

D. Validity of calibration in e⁺-noble gas atom scattering

In this subsection, we examine the formulations described in the previous subsection for e⁺+Ne potential scattering and demonstrate the validity of the calibration modification.

We first investigate the influence of each eigenenergy pair on the phase shifts and examine the validity of Eq. (31). We use the same calculation for the e⁺+Ne potential scattering presented in Sec. III A, i.e., $\theta = 0.25$. Figure 7(a) shows that $\Delta_{x,k}$, $\Delta_{y,k}$, $\Delta_{0x,k}$, and $\Delta_{0y,k}$ of e⁺+Ne potential scattering at $E_{\text{col}} = 0$ eV. $|\Delta_{x,k}|$ and $|\Delta_{y,k}|$ are in the range of 10^{-4}–10^0, while $|\Delta_{0x,k}|$ and $|\Delta_{0y,k}|$ are smaller than 10^{-10}. It is convincing that small $|\Delta_{0x,k}|$ and $|\Delta_{0y,k}|$ because the $\{E_{0,k}\}$, eigenenergies of H_0 (containing only the kinetic energy operator), are on the 2θ line. In contrast, $\{E_k\}$ deviates from the 2θ line owing to the presence of the potential energy operator $V_{\text{e⁺Ne}}$.

In Fig. 7(b), we examine Eq. (30), calculated using $\Delta_{(0)x,k}$ and $\Delta_{(0)y,k}$. The first-order term and first plus second-order term of $\delta_{\text{diff},k}$ are compared with the exact $\delta_{\text{diff},k}(E_{\text{col}} = 0)$. The first-order perturbation makes a dominant contribution to the exact $\delta_{\text{diff},k}$. Including up to the second-order terms, the exact $\delta_{\text{diff},k}$ is almost entirely explained. As the first-order term does not depend on E_{col}, it is convincing that the gross structure of $\delta_{\text{diff},k}$ does not show collision-energy dependence. Thus, the expansion of Eq. (30) is reasonable, and according to Eq. (31), for $\delta_{\text{diff},k}$, the high-energy eigenenergy pairs can be considered as constants compared to E_{col} for low-energy scattering.

Figure 8 presents a comparison of $\delta_{\text{diff},k}$ of e⁺+Ne potential scattering at $E_{\text{col}} = 0$ eV with several collision energies
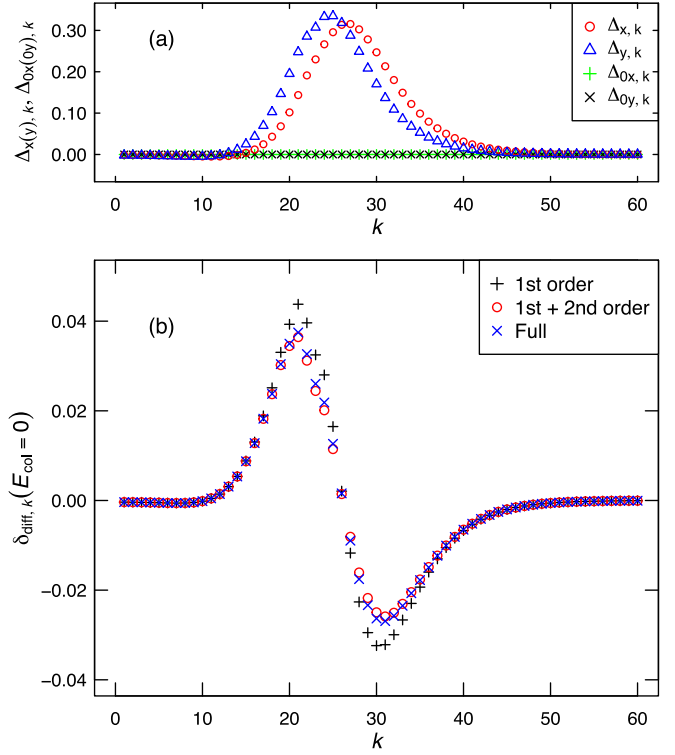

FIG. 7. (a) $\Delta_{x,k}$, $\Delta_{y,k}$, $\Delta_{0x,k}$, and $\Delta_{0y,k}$ of eigenenergies of e⁺+Ne scattering corresponding to Fig. 8. (b) Reproducibility of $\delta_{\text{diff},k}$ (at $E_{\text{col}} = 0$) by the first- and second-order terms calculated from $\Delta_{x,k}$, $\Delta_{y,k}$, $\Delta_{0x,k}$, and $\Delta_{0y,k}$ according to Eq. (30).

$E_{\text{col}} = 0.01, 0.1, 1,$ and 10 eV. The largest $|\delta_{\text{diff},k}|$ for the $E_{\text{col}} = 0$ eV collision is the eigenenergy pair near $k = 20$ and 30. It should be noted that these positive and negative values of $|\delta_{\text{diff},k}|$ totally cancel out and result in zero. The phase shift for $E_{\text{col}} > 0$ is equivalent to the sum of the differences between $\delta_{\text{diff},k}(E_{\text{col}})$ and $\delta_{\text{diff},k}(E_{\text{col}} = 0)$. For each $\delta_{\text{diff},k}(E_{\text{col}})$, a deviation of $\delta_{\text{diff},k}(E_{\text{col}})$ from $E_{\text{col}} = 0$ can be observed around the E_{col}, as expected. For example, the remarkable difference of $\delta_{\text{diff},k}(E_{\text{col}})$ between $E_{\text{col}} = 0$ eV and $E_{\text{col}} = 0.01$ eV can be observed at $\operatorname{Re} E_k = 0.009$ eV, which is close to E_{col}. This is also true for $E_{\text{col}} = 0.1$ and $E_{\text{col}} = 10$ eV. $\delta_{\text{diff},k}$ for $E_{\text{col}} = 1$ eV is very similar to that for $E_{\text{col}} = 0$, which is because $E_{\text{col}} = 1$ eV is close to the Ramsauer-Townsend minimum, where the phase shift becomes zero. In summary, the energy dependence of the phase shift originates from the eigenenergy pairs near the collision energy. Equation (9) formally requires all the eigenenergy pairs, while the eigenenergy pairs far from the collision energy have the same contribution as $E_{\text{col}} = 0$. Thus, Fig. 8 clearly demonstrates the validity of the modification in Eq. (34).

Figure 9 presents the e⁺+Ne S-wave scattering phase shifts obtained using only the lowest 10, 20, and 25 eigenenergy pairs of the 60 pairs in total. As shown in Fig. 9(a), the use of a limited number of eigenenergy pairs results in a nonzero phase shift at $E_{\text{col}} = 0$. However, the "calibrated" phase shifts reproduced the exact phase-shift behavior of low-energy collisions for $n = 14, 18,$ and 22. As the number of eigenenergy pairs increases, the collision energy range, where the "calibrated" phase shifts reproduce the exact phase shifts, becomes wider.
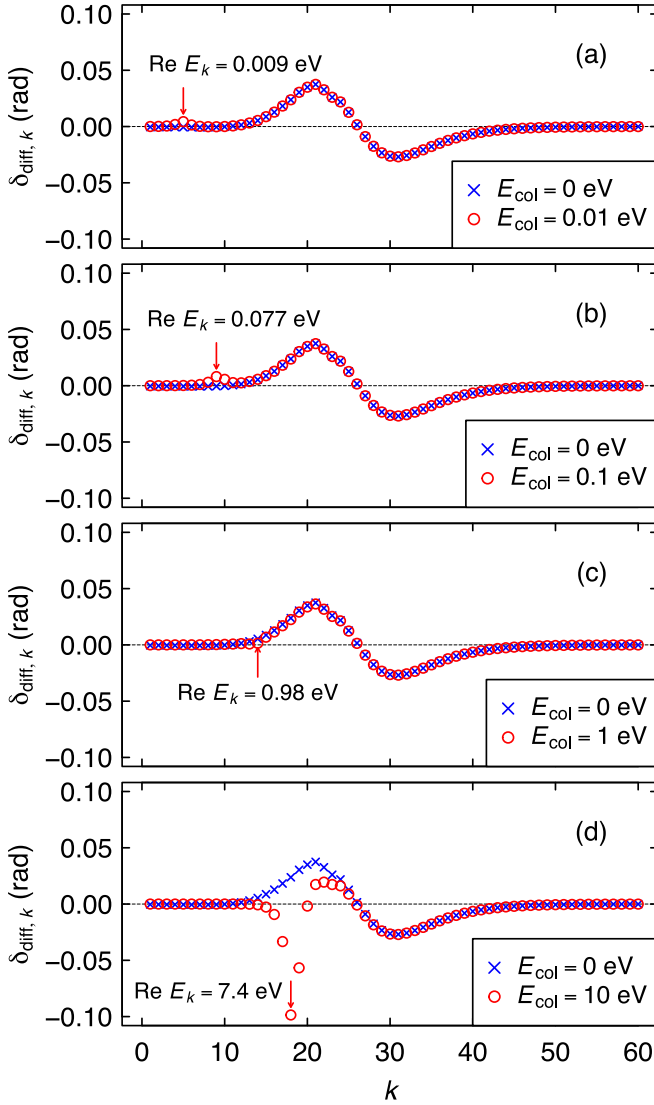
FIG. 8. S-wave phase shift of $e^+ + Ne$ decomposed into $\delta_{\mathrm{diff},k}$ [see Eq. (24) for definition] for each pair of the complex eigenenergies. $E_{\mathrm{col}} = 0.01, 0.1, 1,$ and 10 eV are compared with $E_{\mathrm{col}} = 0$ eV.

Using this modification, the elastic cross sections of $e^+ +$ X (X = Ne, Ar, Kr, Xe) are calculated as shown in Fig. 10. In these calculations, a pair of eigenenergies that satisfies $\mathrm{Re}\, E_{(0,)k} \leqslant E_{\mathrm{cut}}$ are used, where $E_{\mathrm{cut}} = 1, 100,$ and 1000 eV. The partial waves are considered from the S-wave ($l = 0$) to $l = 8$ for Ne, Ar, and Kr, and to $l = 11$ for Xe such that the cross sections converge against the partial waves. With an increase in the number of eigenenergy pairs used for the calculation, the total elastic cross sections reproduced the exact ones calculated using the Numerov method. The indicator $\mathrm{Re}\, E_{0,k_{\max}}/2$ also agrees well with the maximum energy at which the modification is valid.

E. Three- and four-body calculations of e^+ scattering using limited number of eigenenergies

Figure 11(a) presents a comparison of the S-, P-, and D-wave phase shifts of $e^+ + He^+(1s)$ with the latest calculations obtained using the Harris-Nesbet variational method [22].
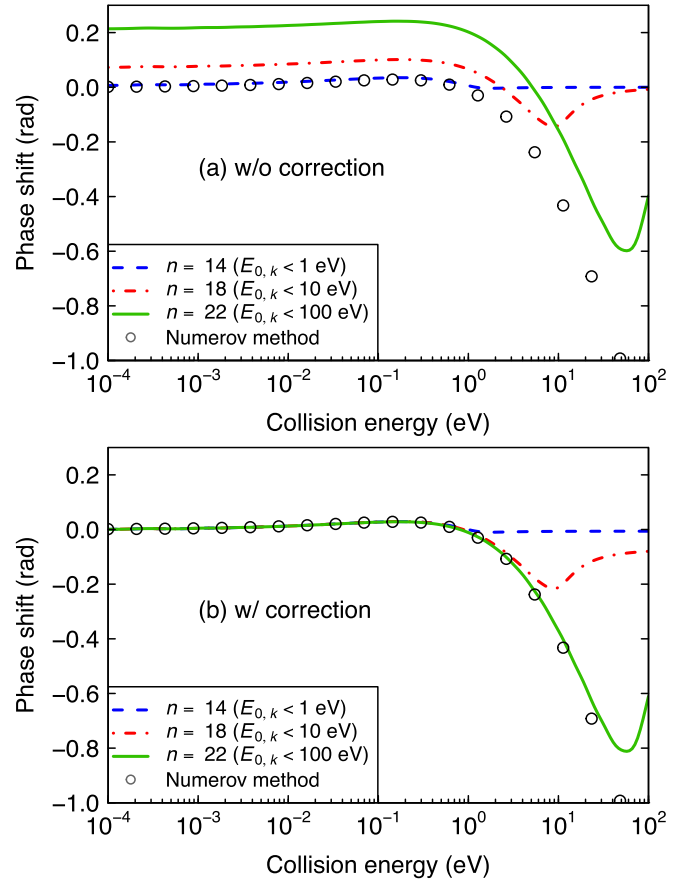

FIG. 9. S-wave phase shifts of $e^+ + Ne$ calculated using a limited number of pairs of complex eigenenergies n. (a) Without calibration and (b) with calibration according to Eq. (34). The phase shifts calculated using the CSM are compared with those calculated using the Numerov method.

We use the complex scaling angle $\theta = 0.15$ rad for S wave, 0.2 rad for P and D waves, include a limited number of eigenenergy pairs (33, 36, and 35 pairs for S, P, and D waves, respectively), and apply the calibration modification for low-energy scattering using Eq. (32). The offsets caused by the modification are -0.01953 rad (S wave), 0.00095 rad (P wave), and 0.00310 rad (D wave). In this calculation, the indicators $\mathrm{Re}\, E_{0,n}/2 - E_{He^+(1s)}$ become 76 eV (S wave), 38 eV (P wave), and 33 eV (D wave). It can be observed that the phase shifts calculated using the complex eigenenergies agree well within the Harris-Nesbet variational calculations. While the D-wave phase shifts present relatively large deviations from the reference at high energies in comparison with the S- and P-wave phase shifts, which is consistent with the smaller $\mathrm{Re}\, E_{0,n}/2 - E_{He^+(1s)}$ than those partial waves.

Figure 11(b) presents the S-wave phase shifts of e^+-He^+ scattering to investigate the number of eigenenergy pairs included in the calculation. When the number of pairs is reduced from 33 to 27, the low-energy behavior of the phase shift remains unchanged, and the high-energy behavior does not match the precise calculation. The 27th eigenenergy corresponds to $\mathrm{Re}\, E_{0,n}/2 - E_{He^+(1s)} = 18$ eV, which is approximately the maximum energy below which the
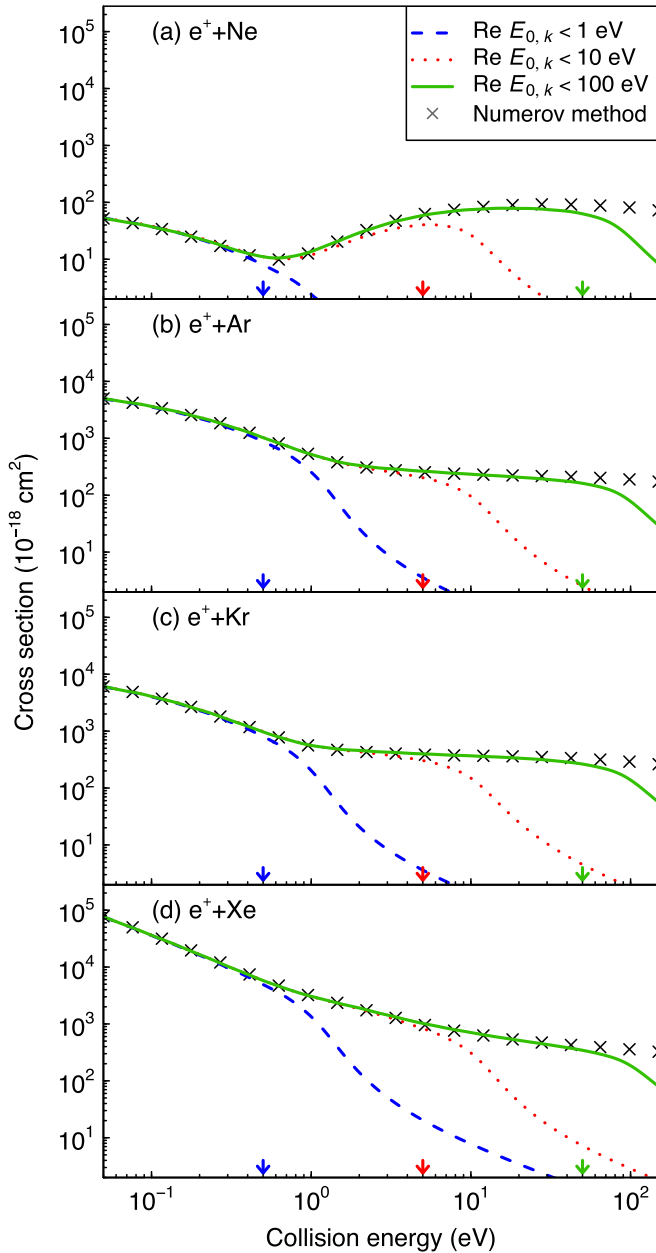
FIG. 10. Elastic scattering cross sections of e+X (X = Ne, Ar, Kr, and Xe) calculated using the calibrated phase shifts are presented against the collision energy. The arrows of colors matching the corresponding line indicate the Re $E_{0,n}/2$, namely, 0.5, 5, 50 eV from left to right, to show the expected applicable range.

FIG. 11. (a) Calibrated phase shifts of the $e^+ + He^+$ scattering compared with those calculated using the Harris-Nesbet (HN) variational method [22]. For each partial wave, we use 33, 36, and 35 pairs of complex eigenenergies for the S, P, and D waves, respectively. The arrows from right to left present the Re$E_{0,n}/2 - E_{He^+(1s)}$ for P and D waves as an indicator of the maximum applicable energy. The Re$E_{0,n}/2 - E_{He^+(1s)}$ for the S wave is located at a much larger energy (approximately 76 eV). (b) The calibrated S-wave phase shifts of the $e^+ + He^+$ scattering calculated using the 33 pairs of complex eigenenergies are compared with those calculated using 27 pairs of complex eigenenergies. The black arrow presents Re$E_{0,k=27}/2 - E_{He^+(1s)}$, which indicates the expected approximation limit for the collision energy.

calculated phase shifts are reliable. This indicator appears to work well for the proposed three-body systems. The advantage of the calibration modification is that only a limited number of eigenenergies are required to determine the phase-shift behavior in low-energy scattering.

Figure 12 summarizes the S-wave phase shifts of e^+-X (X = H, He, He$^+$, Li$^+$, and Li^{2+}) scattering calculated using the CSM with a calibration modification (the complex scaling angle is 0.2 rad for all of the calculations). In general, the phase shift increases as the collision energy increases from zero and then decreases. The low-energy increase mainly originates from the attractive induced dipole interaction between
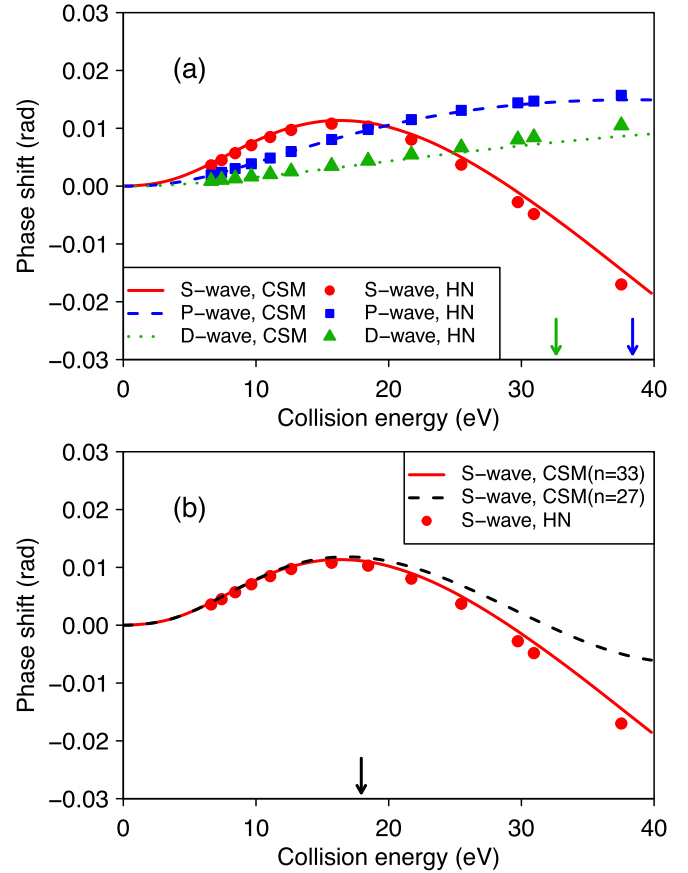
the target atom or ion and the positron, and the decrease at higher energies is attributed to the positron-nucleus repulsive interaction. As observed in this figure, the phase shift behavior of the positron-neutral atom scattering significantly differs from that of the positron-ion scattering owing to the presence of a long-range repulsive Coulomb force in the later case. We emphasize that the CSM calculation successfully describes these different phase-shift behaviors and reproduces the results of previous studies using different methods.

We also predict the phase shift of e^+-Li$^+$ scattering using the same quality of calculation as e^+-He scattering. The obtained phase shift exhibited a similar but more moderate behavior than e^+-He$^+$, which is convincing because an increase in the nuclear charge prevents the positrons from approaching the electrons and reduces the attractive interactions
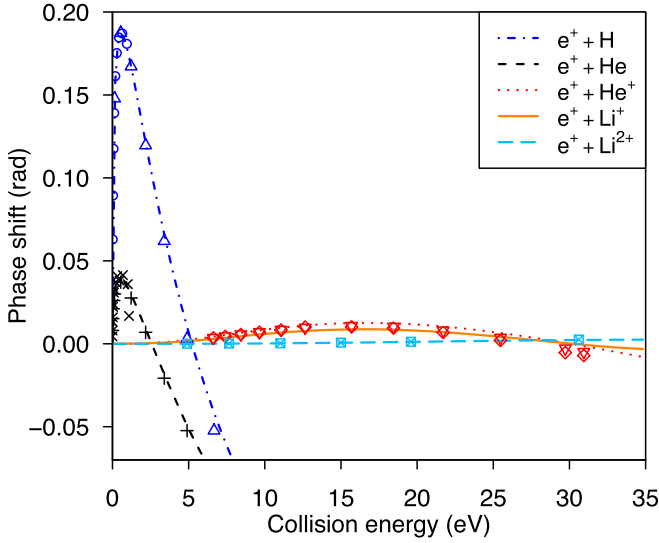
FIG. 12. S-wave phase shifts of positron scattering off H, He, He$^+$, Li$^+$, and Li^{2+} atoms and ions are calculated using the CSM with calibration modification (solid lines). Points denote the previous works: ○ [38] and △ [39] for e$^+$-H, + [40] and × [38] for e$^+$-He, ◇ [21] and ▽ [22] for e$^+$-He$^+$, and ⊠ [41] for e$^+$-Li^{2+}.

between them. A similar trend can be observed in e$^+$-H and e$^+$-He, where the second case shows more moderate behavior. Tables I and II list the numerical values of the S-wave phase shifts of the positron-scattering off the positive ions. Our calculation is denoted as CSM$_{l_{max}}$, where l_{max} indicates the maximum inner angular momenta, l and L in Eqs. (19) and (22), used for the basis functions. With an increase in l_{max}, the phase shifts converge in the presented energy range for the e$^+$ + He$^+$ and e$^+$ + Li^{2+} collisions. In the case of e$^+$ + He$^+$ collisions, the converged values are slightly larger than those reported in the latest literature [21,22]. Similar trends are observed in the case of the e$^+$ + Li^{2+} collisions.

TABLE II. S-wave phase shifts of e$^+$+Li^{2+} collision is compared with the literature values. Our calculations are performed with $\theta = 0.2$ rad and noted as CSM$_{l_{max}}$. CIKOHN$_8$ is referred to for Ref. [42].

k (a.u.)	CSM$_3$	CSM$_2$	CSM$_1$	Novikov [42]	Gien [41]
0.5	1.35[−4]	1.36[−4]	1.28[−4]	1.48[−5]	
0.6	2.17[−4]	2.17[−4]	2.06[−4]		3.68[−5]
0.75	4.12[−4]	4.12[−4]	3.93[−4]		1.20[−4]
0.9	7.49[−4]	7.48[−4]	7.17[−4]		3.13[−4]
1.0	1.09[−3]	1.09[−3]	1.04[−3]	5.39[−4]	
1.05	1.30[−3]	1.29[−3]	1.25[−3]		6.79[−4]
1.2	2.08[−3]	2.08[−3]	2.01[−3]		1.24[−3]
1.5	4.01[−3]	4.01[−3]	3.90[−3]	2.57[−3]	2.55[−3]

Our calculation of CSM$_3$ for e$^+$ + Li^{2+} results in phase shifts a few times larger than those reported in the literature [41,42]. The larger evaluated phase shift at low energies than that in the previous studies indicates that the interaction between the positron and ions is described in a more attractive manner in our calculations. Because the size of our basis functions is relatively large (10 852 at maximum), the description could be improved by including virtual target excitation and virtual Ps formation in comparison with previous calculations. Another possible reason for the deviation from the literature values is the insufficiency of the completeness relationship Eq. (4). In two-body potential scattering, the positron scattering wave function, in principle, satisfies the completeness relationship. However, in few-body scattering, the positron wave function is coupled with the target ion states, including their virtual excitation. The contributions of the virtually excited states of the target ion depend on the collision energy, which can lead to an insufficiency in the completeness relationship. Thus, more careful investigations are required to determine the origin of the small differences in the phase shifts between the CSM calculations and other methods.

TABLE I. S-wave phase shifts of e$^+$+He$^+$ and e$^+$+Li$^+$ collisions calculated by CSM with $\theta = 0.2$ rad. $x[y]$ denotes $x \times 10^y$. Literature values are compared for e$^+$+He$^+$. Our calculations are noted as CSM$_{l_{max}}$, where l_{max} is the maximum inner angular momentum used for the basis functions in this work.

	e$^+$+He$^+$								e$^+$+Li$^+$
E_{col}(eV)	CSM$_3$	CSM$_2$	CSM$_1$	CSM$_0$	Gien [22]	Bransden [21]	Khan [20]	Shimamura [19]	CSM
6.62	4.56[−3]	4.56[−3]	4.48[−3]	1.42[−3]	3.59[−3]	3.56[−3]	3.40[−3]	1.50[−3]	3.23[−3]
7.41	5.61[−3]	5.60[−3]	5.50[−3]	1.78[−3]	4.50[−3]	4.46[−3]	4.20[−3]	2.40[−3]	3.94[−3]
8.43	6.97[−3]	6.97[−3]	6.85[−3]	2.27[−3]	5.70[−3]	5.60[−3]	5.20[−3]	4.00[−3]	4.92[−3]
9.65	8.55[−3]	8.55[−3]	8.41[−3]	2.85[−3]	7.08[−3]	6.95[−3]	6.40[−3]	5.60[−3]	6.06[−3]
11.07	1.02[−2]	1.02[−2]	1.00[−2]	3.45[−3]	8.49[−3]	8.29[−3]	7.40[−3]	7.00[−3]	7.23[−3]
12.65	1.17[−2]	1.17[−2]	1.15[−2]	3.93[−3]	9.72[−3]	1.01[−2]	8.00[−3]	7.80[−3]	8.28[−3]
15.7	1.33[−2]	1.33[−2]	1.31[−2]	4.10[−3]	1.08[−2]	1.02[−2]	7.90[−3]	6.60[−3]	9.35[−3]
18.45	1.33[−2]	1.33[−2]	1.31[−2]	3.28[−3]	1.03[−2]	9.42[−3]	6.30[−3]	6.30[−3]	9.18[−3]
21.71	1.17[−2]	1.16[−2]	1.15[−2]	1.16[−3]	8.03[−3]	6.80[−3]	2.70[−3]	4.40[−3]	7.67[−3]
25.47	8.06[−3]	8.05[−3]	7.86[−3]	−2.61[−3]	3.67[−3]	2.01[−3]	–	6.00[−4]	4.55[−3]
29.73	2.44[−3]	2.43[−3]	2.24[−3]	−8.13[−3]	−2.81[−3]	−5.32[−3]	−1.07[−2]	−5.40[−3]	−1.65[−4]
30.94	6.42[−4]	6.32[−4]	4.37[−4]	−9.87[−3]	−4.88[−3]	−7.10[−3]	−1.31[−2]	−1.03[−2]	−1.65[−3]
37.53	−1.00[−2]	−1.00[−2]	−1.03[−2]	−2.02[−2]	−1.70[−2]	−1.97[−2]	−2.68[−2]	−2.18[−2]	−9.43[−3]

IV. CONCLUSION

We presented the phase-shift calculation of e^+-X scattering using CSM for the targets X = Ne, Ar, Kr, Xe, H, He, He^+, Li^{2+}, and Li^+. We observed the empirical fact that a complex eigenenergy pair whose real part was much greater than the collision energy was required to achieve the convergence of the phase shift, even for low-energy scattering. Although the necessity for these high-lying complex eigenenergies may result in difficulties in few-body problems, the contribution of these high-lying complex eigenenergies to the phase shift can be regarded as a constant, and we proposed a modification to the CSM calculation. The use of the modification was suggested by the simple geometrical considerations described in Sec. III C. The validity of the modification was demonstrated by the positron scattering off X = Ne, Ar, Kr, Xe, H, He, He^+, and Li^{2+}, which was in good agreement with the literature. We predicted the phase shifts of the e^+-Li^+ four-body scattering problem.

It should be noted that the present formulation of the phase-shift calculation was employed only on the complex energy plane. It was intriguing that the use of CSM converted the quantum mechanical scattering problem into a problem of simple geometry on a complex energy plane. This may provide insights into scattering problems in future studies. While the demonstrated cases presented in this study were limited to the elastic scattering of the system having no resonance or bound state, more general formulations for a variety of systems, including resonance scattering and/or inelastic scattering, will be focused on in future works. Positronium scattering off atoms, ions, and molecules below its breakup threshold that was investigated in recent experiments [13] and theoretical development [38,43–45] would also be in the scope of this approach.

ACKNOWLEDGMENTS

APPENDIX: EXPANSION OF δ_k AND EXPLICIT FORM OF a_k AND b_k

Here, we describe the explicit expressions for a_k and b_k in Eq. (31). δ_k in Eq. (10) can be written as

$$\delta_k = \tan^{-1}\left(\tan(2\theta)\frac{1 + \Delta_{y,k}}{1 + \tilde{\Delta}_{x,k}}\right). \quad (A1)$$

The CSM calculation using $\theta < \pi/4$ (typically approximately $\pi/12$) ensures that $\tan(2\theta) < 1$. As explained in the main text, $\Delta_{y,k} \ll 1$ and $\tilde{\Delta}_{x,k} \ll 1$. The Taylor expansion is applied to $(1 + \tilde{\Delta}_{x,k})^{-1} = 1 - \tilde{\Delta}_{x,k} + \tilde{\Delta}_{x,k}^2 - \cdots$ and the Maclaurin expansion of $\tan^{-1}[z(1 + \Delta)]$, where $z(1 + \Delta) < 1$ and $\Delta \ll 1$,

$$\tan^{-1}[z(1 + \Delta)]$$
$$= \tan^{-1}(z) + \frac{z}{z^2 + 1}\Delta - \frac{z^3}{(z^2 + 1)^2}\Delta^2 + \cdots, \quad (A2)$$

we have Eq. (29). Thus, the explicit forms of a_k and b_k are given as

$$a_k = \tfrac{1}{2}\sin(4\theta)\big\{-\Delta_{x,k} + \Delta_{0x,k} + \Delta_{y,k} - \Delta_{0y,k} + \cos^2(2\theta)$$
$$\times \big(\Delta_{x,k}^2 - \Delta_{x,k}'^2\big) - \cos(4\theta)(\Delta_{x,k}\Delta_{y,k} - \Delta_{0x,k}\Delta_{0y,k})$$
$$- \sin^2(2\theta)\big(\Delta_{y,k}^2 - \Delta_{y,k}'^2\big)\big\}, \quad (A3)$$

and

$$b_k = \tfrac{1}{2}\sin(4\theta)\{-2\cos^2(2\theta)(\Delta_{x,k} - \Delta_{0x,k})$$
$$+ \cos(4\theta)(\Delta_{y,k} - \Delta_{0y,k})\}. \quad (A4)$$

In the evaluation of $|a_k \mathrm{Re}\, E_{0,k}/b_k|$ of Eq. (35), there exists an exceptional case wherein $\Delta_{x,k} - \Delta_{0x,k} \approx \Delta_{y,k} - \Delta_{0y,k}$. In this case, b_k should be smaller than $a_i (i < k)$, and $\delta_{\mathrm{diff},k}$ would have negligible contribution to the sum of $a_i (i < k)$.

[1] A. S. Kadyrov and I. Bray, Phys. Rev. A **66**, 012710 (2002).

[2] D. V. Fursa and I. Bray, New J. Phys. **14**, 035002 (2012).

[3] M. R. Natisin, J. R. Danielson, and C. M. Surko, Phys. Plasmas **22**, 033501 (2015).

[4] M. R. Natisin, J. R. Danielson, and C. M. Surko, Appl. Phys. Lett. **108**, 024102 (2016).

[5] G. F. Gribakin, J. A. Young, and C. M. Surko, Rev. Mod. Phys. **82**, 2557 (2010).

[6] L. Chiari and A. Zecca, EPJ D **68**, 297 (2014).

[7] K. Ratnavelu, M. J. Brunger, and S. J. Buckman, J. Phys. Chem. Ref. Data **48**, 023102 (2019).

[8] J. R. Machacek, S. J. Buckman, and J. P. Sullivan, Rev. Sci. Instrum. **91**, 033311 (2021).

[9] M. H. Rayment, L. Gurung, R. E. Sheldon, S. D. Hogan, and D. B. Cassidy, Phys. Rev. A **100**, 013410 (2019).

[10] K. Michishio, L. Chiari, F. Tanaka, N. Oshima, and Y. Nagashima, Rev. Sci. Instrum. **90**, 023305 (2019).

[11] Y. Nagashima, K. Michishio, L. Chiari, and Y. Nagata, J. Phys. B: At., Mol. Opt. Phys. **54**, 212001 (2021).

[12] S. J. Brawley, S. Armitage, J. Beale, D. E. Leslie, A. I. Williams, and G. Laricchia, Science **330**, 789 (2010).

[13] S. J. Brawley, S. E. Fayer, M. Shipman, and G. Laricchia, Phys. Rev. Lett. **115**, 223201 (2015).

[14] I. I. Fabrikant and G. F. Gribakin, Phys. Rev. A **90**, 052717 (2014).

[15] A. R. Swann and G. F. Gribakin, Phys. Rev. A **97**, 012706 (2018).

[16] T. Yamashita, Y. Kino, E. Hiyama, S. Jonsell, and P. Froelich, Phys. Rev. A **105**, 052812 (2022).

[17] T. Yamashita, Y. Kino, E. Hiyama, S. Jonsell, and P. Froelich, Few-Body Syst. **62**, 81 (2021).

[18] T. Yamashita, Y. Kino, E. Hiyama, S. Jonsell, and P. Froelich, New J. Phys. **23**, 012001 (2021).

[19] I. Shimamura, J. Phys. Soc. Jpn. **31**, 217 (1971).

[20] P. Khan, P. S. Mazumder, and A. S. Ghosh, Z. Phys. A **318**, 19 (1984).

[21] B. H. Bransden, C. J. Noble, and R. J. Whitehead, J. Phys. B: At., Mol. Opt. Phys. **34**, 2267 (2001).

[22] T. T. Gien, J. Phys. B: At., Mol. Opt. Phys. **34**, L535 (2001).

[23] Y. Ho, Phys. Rep. **99**, 1 (1983).

[24] R. Suzuki, T. Myo, and K. Katō, Prog. Theor. Phys. **113**, 1273 (2005).

[25] R. Suzuki, A. T. Kruppa, B. G. Giraud, and K. Katō, Prog. Theor. Phys. **119**, 949 (2008).

[26] M. Odsuren, K. Katō, M. Aikawa, and T. Myo, Phys. Rev. C **89**, 034322 (2014).

[27] M. Odsuren, T. Myo, Y. Kikuchi, M. Teshigawara, and K. Katō, Phys. Rev. C **104**, 014325 (2021).

[28] E. Hiyama, Y. Kino, and M. Kamimura, Prog. Part. Nucl. Phys. **51**, 223 (2003).

[29] B. Giraud and K. Katō, Ann. Phys. **308**, 115 (2003).

[30] B. G. Giraud, K. KatÅ, and A. Ohnishi, J. Phys. A: Math. Gen. **37**, 11575 (2004).

[31] S. Shlomo, Nucl. Phys. A **539**, 17 (1992).

[32] R. D. Levine, *Quantum Mechanics of Molecular Rate Processes* (Clarendon Press, Oxford, 1969), p. 101106.

[33] T. Tsang and T. Osborn, Nucl. Phys. A **247**, 43 (1975).

[34] T. Osborn and T. Tsang, Ann. Phys. **101**, 119 (1976).

[35] F. Salvat, J. D. Martiu inez, R. Mayol, and J. Parellada, Phys. Rev. A **36**, 467 (1987).

[36] F. Arretche, M. V. Barp, W. Tenfen, and E. P. Seidel, Braz. J. Phys. **50**, 844 (2020).

[37] D. Basu, S. K. Datta, P. Kahn, and A. S. Ghosh, Phys. Rev. A **35**, 5255 (1987).

[38] J. Y. Zhang and J. Mitroy, Phys. Rev. A **78**, 012703 (2008).

[39] A. K. Bhatia, A. Temkin, R. J. Drachman, and H. Eiserike, Phys. Rev. A **3**, 1328 (1971).

[40] D. G. Green, J. A. Ludlow, and G. F. Gribakin, Phys. Rev. A **90**, 032712 (2014).

[41] T. T. Gien, J. Phys. B: At., Mol. Opt. Phys. **34**, 5103 (2001).

[42] S. A. Novikov, M. W. J. Bromley, and J. Mitroy, Phys. Rev. A **69**, 052702 (2004).

[43] M.-S. Wu, J.-Y. Zhang, X. Gao, Y. Qian, H.-H. Xie, K. Varga, Z.-C. Yan, and U. Schwingenschlögl, Phys. Rev. A **101**, 042705 (2020).

[44] M.-S. Wu, J.-Y. Zhang, Y. Qian, K. Varga, U. Schwingenschlögl, and Z.-C. Yan, Phys. Rev. A **103**, 022817 (2021).

[45] A. R. Swann, D. G. Green, and G. F. Gribakin, Phys. Rev. A **107**, 042802 (2023).